IEEE Access
Multidisciplinary ⋮ Rapid Review ⋮ Open Access Journal

Received 29 July 2023, accepted 14 August 2023, date of publication 21 August 2023, date of current version 30 August 2023.

Digital Object Identifier 10.1109/ACCESS.2023.3306950

RESEARCH ARTICLE

Reconfigurable THz Fixed-Frequency Beamscanning Through a Liquid-Crystal-Loaded Leaky Waveguide Operating in Its Fundamental TE Mode

WALTER FUSCALDO[1], (Senior Member, IEEE), ELAHEHSADAT TORABI[2], DIMITRIOS C. ZOGRAFOPOULOS[1], DANILO ERRICOLO[2], (Fellow, IEEE), AND ROMEO BECCHERELLI[1], (Member, IEEE)

[1]Istituto per la Microelettronica e Microsistemi, Consiglio Nazionale delle Ricerche, 00133 Rome, Italy
[2]Electrical and Computer Engineering, University of Illinois at Chicago, Chicago, IL 60607, USA

Corresponding author: Dimitrios C. Zografopoulos (dimitrios.zografopoulos@cnr.it)

This work was supported in part by the Project ''Ecosistemi dell'Innovazione''–Rome Technopole of the Italian Ministry of University and Research (public call n. 3277, Piano Nazionale di Ripresa e Resilienza (PNRR)–Mission 4, Component 2, Investment 1.5) funded by the European Union, Next GenerationEU, under Grant ECS00000024.

ABSTRACT A rectangular metallic leaky waveguide loaded with liquid crystals (LC) and operating in its fundamental TE mode at 1 THz is proposed to mitigate the well-known trade-off between directivity and tunable angular range of dynamic beamscanning antennas. The radiating aperture consists of a partially reflecting sheet (PRS) realized through a one-dimensional array of longitudinal slots etched on one of the metallic walls of the waveguide to efficiently couple with the propagating TE leaky mode. The antenna performance is evaluated by defining suitable figures of merit that take into account the beamscanning feature and the gain peak. These figures of merit are evaluated for different combinations of the antenna design parameters. After optimization, a tunable angular range of about 28° is reached, while maintaining a gain of around 7 dBi. A leaky-wave analysis of a simplified model of the structure allows to design the antenna without resorting to computationally expensive optimization processes. More rigorous models are then considered to accurately analyze the LC dynamics and the radiating properties of the PRS. The three-dimensional structure is finally validated through full-wave simulations, showing a remarkable agreement with the theoretical predictions obtained with the simplified model.

INDEX TERMS Directive antennas, leaky-wave antennas, leaky waves, liquid crystals, terahertz radiation, tunable circuits, devices.

I. INTRODUCTION

Terahertz (THz) radiation is attractive in several application contexts thanks to its non-ionizing character, its short wavelengths (0.03 mm to 3 mm), and its potential for establishing communications over wide frequency bandwidths. These properties have led to ever-growing THz applications such as medical diagnosis, pharmaceutical control, high-resolution imaging, material characterization, security, astrophysics, and communications [1], [2], [3], [4], [5], [6], [7].

Still, THz technology presents a number of shortcomings such as low energy radiation and small effective area [8]. Such limitations can be overcome by focusing the THz radiated power in a narrow beam that is eventually steered over a wide angular range. This possibility is of crucial importance e.g., in next-generation ultrafast indoor/short-range multi-user wireless networks since focusing and directing the beam improves the signal-to-noise ratio at the receiver, and therefore the coverage for a given radiated power. In addition, the

The associate editor coordinating the review of this manuscript and approving it for publication was Debabrata K. Karmokar.

beamsteering capability may be exploited to replace multiple antennas with one, and thus reduce the number of components, hardware complexity, and cost [9].

Beamsteering THz antennas have been demonstrated by different approaches (a recent and exhaustive review can be found in [10]) such as electromechanical scanning [11], phased-arrays [12], multibeam switching technology [13], reconfigurable and field-programmable metasurfaces [14] and frequency-scanning leaky-wave antennas (LWAs) [15]. The latter are faster and more precise in beamsteering than methods involving mechanical scanning. Besides, compared to other electrical solutions, they offer a simple feeding and beamsteering mechanism. Interestingly, LWAs also offer the possibility to achieve two-dimensional (2-D) frequency-scanning at THz when arranged in one-dimensional (1-D) arrays as recently shown in [16] where a true-time-delay phasing technique has been applied.

LWAs consist of a partially open waveguide which leaks power into free space as a perturbed guided wave (a *leaky* wave) that travels along the axis of propagation [17], [18]. This power leakage depends on the complex propagation constant $k_z = \beta - j\alpha$ of the dominant leaky mode, with β and α the *leaky* phase and attenuation constants, respectively. In LWAs, the leaky phase constant β is directly related to the angle of radiation and depends on frequency, thus all LWAs have an intrinsic frequency-scanning character. By exploiting this mechanism, beamsteering at a *fixed frequency* can also be achieved, by dynamically controlling β. Indeed, the phase constant can be affected in several ways, e.g., by changing the electromagnetic properties of the materials composing the LWA. For instance, one may use tunable materials such as graphene or liquid crystals (LCs).

Graphene has been vastly studied as a tunable element to realize THz aborbers (see, e.g., [19], [20]), and as a tunable partially reflecting sheet (PRS) for realizing THz LWAs (see, e.g., [21], [22], [23]). Conversely, LCs were less investigated at THz although their performance improves drastically at such frequencies compared to millimeter-wave and microwave frequencies [24], as they are closer to the natural range of operation of LCs, namely the visible and near infrared parts of the electromagnetic spectrum [25], [26]. In this respect, LCs offer an advantageous alternative for continuous dynamical tuning compared to traditional solutions such as PIN diodes and varactors, whose performance rapidly deteriorates for frequencies deeper in the THz spectrum. Moreover, smaller wavelengths allow for smaller LC cavities and thus more compact devices with a faster response time, which is typically inversely proportional to the square of the LC cavity thickness, and lower power consumption and cost [27], [28], [29], [30], [31].

In the W-band (i.e., 75 GHz to 110 GHz), an image-line LC-based LWA has been recently fabricated and measured, showing an electrical scanning range of about 10° and average gain of about 12 dBi [31]. At higher frequencies, around 1 THz, a waveguide-based 1-D LWA has recently been proposed on a theoretical basis [32]. The waveguide was partially filled with an LC material sandwiched between two layers of low-loss polymer (Zeonor(R)) and polarized through a bias voltage applied between the bottom ground plane and the top patterned metallic plate. The biasing scheme required the waveguide to operate with the fundamental TM mode, which in turn needed a perfect magnetic conductor (PMC) at the lateral walls. The PMC walls were synthesized with a 2-D array of subwavelength patches that behave as a PMC in a very narrow bandwidth centered around the operating frequency of 1.05 THz. A 1-D array of transverse slots was patterned on the aperture plane to effectively couple with the propagating TM mode and allow for radiation. Although full-wave simulations demonstrated interesting beamsteering capabilities (about 15° of steering at 1.05 THz with an average gain of 12 dBi), the use of the TM mode in such 1-D LWAs poses challenges in terms of fabrication and biasing and limits its tunability and bandwidth performance, thus calling for different designs and physics-oriented optimization models capable of improving the antenna perfomance.

As a considerable step forward, we thoroughly investigate a THz 1-D LWA based on LC and PRS working on its fundamental TE mode, which allows to replace the PMC walls with perfect electric conductor (PEC) walls [33]. As a result, the structure consists of a significantly simpler rectangular metallic waveguide partially filled with an LC, where one of the walls is replaced by a PRS (here a 1-D array of longitudinal slots) to allow for radiation. In the proposed configuration, the LC bias voltage is applied across the LC cell, without the voltage drop across the Zeonor layers experienced by the previous PMC based design; this greatly reduces the driving voltage. Moreover, we defined suitable figures of merit to run an original optimization process (by properly selecting the PRS impedance and LC thickness) capable of realizing an optimum trade-off between average gain and angular range, namely 7 dBi and 28°, respectively, at around 1 THz. Such an optimization considerably differs from those proposed for more common 1-D LWAs [34], [35] that are not capable to deal with tunable, anisotropic materials, such as LC.

The manuscript is organized as follows. First, we describe the antenna structure and present its equivalent circuit model (Section II). Approximate analytical formulas and numerical means are then used to design the antenna for maximum gain and beam steering (Section III). The synthesis of the aperture distribution through a 1-D array of longitudinal slots is discussed (Section IV) along with the description of the LC dynamics under biasing conditions (Section V). Full-wave results are reported to validate the entire analysis (Section VI). Finally, conclusions are drawn (Section VII).

II. ANTENNA STRUCTURE AND MODEL

A. ANTENNA OVERVIEW

The antenna architecture of the proposed 1-D LWA is sketched in Fig. 1. The waveguide cross section consists of three dielectric layers, namely one LC layer sandwiched between two spacers, bounded by three PEC walls and a PRS.

The crucial difference between the two structures is due to the presence here of the PEC side walls in place of the PMC side walls in [32], which greatly improves the LC dynamics (see Section V), simplifies the manufacturing process and improves the compactness of the device.

Hence, there is a need for a specific different dispersion analysis and optimization process (TE leaky modes have to be studied instead of TM leaky modes) that will be soon discussed. The LC control bias is applied between the two PEC walls of the leaky waveguide as shown in Fig. 1(a). The two walls are electrically disconnected from the other conducting walls in the waveguide as discussed in Section V.

The spacers are realized with Zeonor, a cyclo-olefin polymer (COP) with a complex THz relative permittivity $\varepsilon_{sp} = 2.3(1 - j0.001)$ that we have chosen for its low absorption loss and low index mismatch with respect to the ordinary refractive index of the LC. The PRS consists of a 1-D periodic array of longitudinal slots that effectively couple with the fundamental TE leaky mode that propagates in the leaky waveguide. The electromagnetic behavior of this kind of PRS can be accurately described by a purely imaginary admittance $Y_s = jB_s$ that will be here used in the numerical and full-wave analysis [35]. More details about the PRS realization and its electromagnetic properties will be given in Section IV.

The employed LC material is the highly-birefringent nematic mixture w-1825, which is characterized by ordinary and extraordinary relative permittivity values of $\varepsilon_\perp = 2.42(1 - j0.08)$ and $\varepsilon_\parallel = 3.76(1 - j0.05)$ around 1 THz, respectively [36]. With reference to the dispersion and radiation analysis and consequent optimization of the LWA, the LC is at first modeled as a uniaxial crystal (a diagonal tensor of relative permittivity). At rest, the LC molecules are aligned parallel to the four interfaces that encapsulate the cavity by means of a rubbed polymer layer as customary to LC technology. The application of a bias voltage will cause the LC molecules to re-orient from the z-axis (parallel to the PEC side walls) to the y-axis (perpendicular to the PEC side walls) which in turn causes the ε_{yy} permittivity tensor diagonal component to switch its value from $\varepsilon_\perp$ to $\varepsilon_\parallel$ (and viceversa for ε_{zz}); this behavior is responsible for the dynamic beamscanning feature of the antenna, as the LC switching modulates the phase constant of the y-polarized TE propagating leaky mode. A more complete and rigorous description of the LC dynamics will be discussed in Section V for the optimized structure. It will be shown that the above-mentioned simplified model is sufficiently accurate to drive the optimization process.

B. DISPERSION EQUATION

In order to optimize the antenna structure, it is necessary to know its radiating performance. When properly designed, the leaky-wave aperture field of a LWA dominates the total aperture field, thus the radiating features are fully determined by the leaky propagation constant, i.e. $k_z = \beta - j\alpha$.

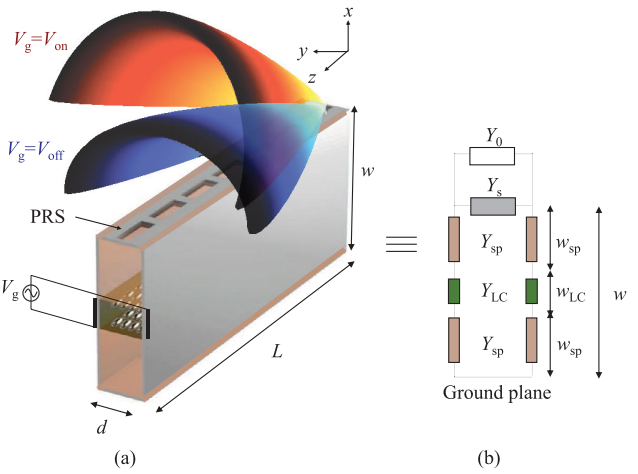

FIGURE 1. (a) Schematic of the design; $w = \lambda_0/(2\sqrt{\mathrm{Re}[\varepsilon_\perp]})$, $w_{sp} = 0.4w$, $w_{LC} = 0.2w$, $d = w/2$, $L = 5\lambda_0$. (b) The equivalent transmission line model.

The complex propagation constant of a leaky rectangular waveguide as the one shown in Fig. 1(a) can be obtained by solving for the improper (i.e., $\mathrm{Im}[k_x] > 0$, see [37], [38], [39]) complex roots of the relevant dispersion equation. The latter can easily be obtained from the application of the transverse resonance technique to the equivalent transmission-line model shown in Fig. 1(b). As discussed in [32], this method leads to the following dispersion equation

$$Y_0 + Y_s + Y_{TL}(Y_{sp}, Y_{LC}) = 0 \tag{1}$$

where Y_0, Y_{sp}, Y_{LC}, represent the wave admittances of air, spacer, and LC media, respectively, and Y_{TL} is the input admittance of the three-section transmission-line terminated with a short circuit representing the ground plane. The expression of Y_{TL} depends on Y_{sp} and Y_{LC}; it can easily be obtained by recursively using the definition of input admittance at each section.

As opposed to the TM case treated in [32], we are here interested in the TE case, thus $Y_0 = 1/(\eta_0\sqrt{k_0^2 - k_z^2})$, $Y_{sp} = 1/(\eta_0\sqrt{k_0^2\varepsilon_{sp} - k_z^2})$, $Y_{LC} = 1/(\eta_0\sqrt{k_0^2\varepsilon_{yy} - k_z^2})$, with η_0 and k_0 the free-space impedance and wavenumber, respectively. Since ε_{yy} is a function of the applied bias voltage (see Section V) the complex roots of (1) will change accordingly.

Root-finding methods such as the Padé algorithm [40] can be employed to obtain the wavenumber dispersion of the TE leaky mode. A good initial guess for the algorithm is obtained by considering the wavenumber dispersion of an equivalent homogenous medium with an effective permittivity $\varepsilon_{eff} = \varepsilon'_{eff}(1 - j\tan\delta_{eff})$ and a loss tangent $\tan\delta_{eq}$

$$k_z \simeq \sqrt{k_0^2\varepsilon'_{eff}(1 - j\tan\delta_{eq}) - \left(\frac{\pi}{w}\right)^2} \tag{2}$$

where w is the cavity height which is set to $w = \lambda_0/(2\sqrt{\varepsilon_\perp})$ with λ_0 the free-space wavelength at the *design* frequency f_0, here chosen equal to 1 THz. In such a way the antenna

will resonate close to f_0 providing radiation close to broadside when maximum bias is applied.

A zeroth-order approximation is used for the complex effective permittivity which is given by

$$\varepsilon_{\text{eff}} = \frac{w - w_{\text{LC}}}{w}\varepsilon_{\text{sp}} + \frac{w_{\text{LC}}}{w}\varepsilon_{yy} \tag{3}$$

whereas the equivalent loss tangent is given by [41]

$$\tan\delta_{\text{eq}} = \tan\delta_{\text{eff}} + \frac{2}{\pi}\frac{\varepsilon'_{\text{eff}}}{1+\eta_0^2 B_{\text{s}}^2} \tag{4}$$

with $\tan\delta_{\text{eff}} := -\text{Im}[\varepsilon_{\text{eff}}/\varepsilon'_{\text{eff}}]$. In conventional LWAs the dispersion equation is typically solved over a given frequency range to show the wavenumber dispersion (in its real and imaginary parts) as a function of frequency. Here, we are interested in the antenna performance at a fixed frequency. Therefore, in the following Section III the dispersion equation will be solved for different values of reactance $X_{\text{s}} = -1/B_{\text{s}}$ and LC volume ratio w_{LC}/w at a fixed frequency.

III. ANTENNA DESIGN

In order to drive an antenna optimization procedure, we need to define the objective functions. Here, the relevant figures of merit are represented by the tunable range $\Delta\theta := |\theta_{0,\text{on}} - \theta_{0,\text{off}}|$, defined as the maximum angular variation between the beam angle in the 'on' and 'off' state of the LC, and the average gain $G_{\text{ave}} = (G_{\text{on}} + G_{\text{off}})/2$, defined as the average gain peak between the two LC states. In the next Subsection II-A, we provide simple analytical formulas to evaluate these figures of merit, whereas in Subsection II-B the results of the numerical optimization process are shown.

A. FIGURES OF MERIT

As is known [34], [42] the radiation power pattern of a finite-length 1-D LWA can be expressed as

$$P(\theta) = \frac{\sinh^2 a + \sin^2 t(\theta)}{a^2 + t(\theta)^2}\cos^2\theta \tag{5}$$

where $a = \alpha L/2$, $t(\theta) = b - l\sin\theta$, $l = k_0 L/2$, $b = \beta L/2$, L, being the antenna length. We note that the cosine squared term appearing in the expression is due to the polarization of the longitudinal radiating current (here, realized through longitudinal slots), which enforces a null at endfire as well as beam narrowing and beam shift effects [43], [44].

From this expression a number of interesting antenna properties can be derived. The beam angle is given by $\theta_0 = \arcsin(\beta/k_0)$ so that the tunable range $\Delta\theta$ can be evaluated as

$$\Delta\theta = |\arcsin(\beta_{\text{on}}/k_0) - \arcsin(\beta_{\text{off}}/k_0)| \tag{6}$$

where $\beta_{\text{on(off)}}$ is the leaky phase constant in the 'on'('off') state of the LC.

The half-power beamwidth Θ_{h} is given by [34]

$$\Theta_{\text{h}} \simeq 2\sec\theta_0 t_{\text{h}}(a)/l \tag{7}$$

with $t_{\text{h}}(a) = 1.39156[1-\tanh(0.021a)] + a\tanh(0.21a)$ [42].

The total efficiency (neglecting the insertion loss) of the LWA is

$$e_{\text{tot}} = e_{\text{ap}}\frac{\alpha_{\text{rad}}\beta_{\text{rad}}}{\alpha\beta} \tag{8}$$

where $e_{\text{ap}} = 1 - e^{-2\alpha L}$ is the aperture efficiency of the LWA, whereas β_{rad} and α_{rad} are the leaky phase and attenuation constants due to radiation loss for a lossless structure. Finally, the gain is easily obtained using the previous expression for the total efficiency and the *corrected* formula for the directivity of 1-D LWAs [34]

$$G \simeq \frac{2e_{\text{tot}}\text{CF}(\beta,\alpha,L)}{(t_{\text{h}}/l)} \tag{9}$$

where CF is a correction function suitable for 1-D LWAs, whose expression is derived in [34] and not reported here for the sake of brevity. From (6) and (9), G_{ave} and $\Delta\theta$ can be evaluated analytically, once the phase and attenuation constants of the leaky mode are known.

It is worthwhile pointing out here that, in conventional LWAs, the gain-bandwidth figure of merit is one of the most used (see [17], [45] and refs. therein). This figure of merit is evidently not appropriate for beamscanning LWAs that work at fixed frequency as the one investigated here. Hence, we define a different figure of merit as the product between the tunable range and the average gain therein:

$$\text{FoM} = \Delta\theta \cdot G_{\text{ave}} \propto e_{\text{tot}}\frac{\Delta\theta}{\Theta_{\text{h}}} \tag{10}$$

where the expression on the right gives another interpretation to the FoM: it is proportional to the product between the total antenna efficiency and the *effective* tunable range, i.e., the tunable range normalized to the beamwidth.

The gain, the tunable range, and the FoM will be the objective functions to be considered during the optimization process, by varying the LC volume ratio and the sheet reactance.

B. OPTIMIZATION

The antenna architecture described in the previous Section II has numerous degrees of freedom, namely the overall waveguide height w, the LC volume ratio w_{LC}/w, the *operating* frequency f_{op}, the sheet reactance X_{s}, and the antenna length L. A full-wave optimization process of the antenna over this 5-D parameter space would be prohibitive in terms of computational resources. On the other hand, the semi-analytical procedure outlined in [35] cannot be applied here due to the presence of a multilayered cross-section with a tunable anisotropic layer (viz., the LC). For this purpose, we propose a different strategy that reduces the number of degrees of freedom under sound physical assumptions.

First, the antenna length L does not play a significant role in the optimization process for a two-fold reason. On one hand, at such short wavelenghts a physical size of just few centimeters corresponds to hundreds of wavelengths. On the other hand, the use of materials with finite losses raises the

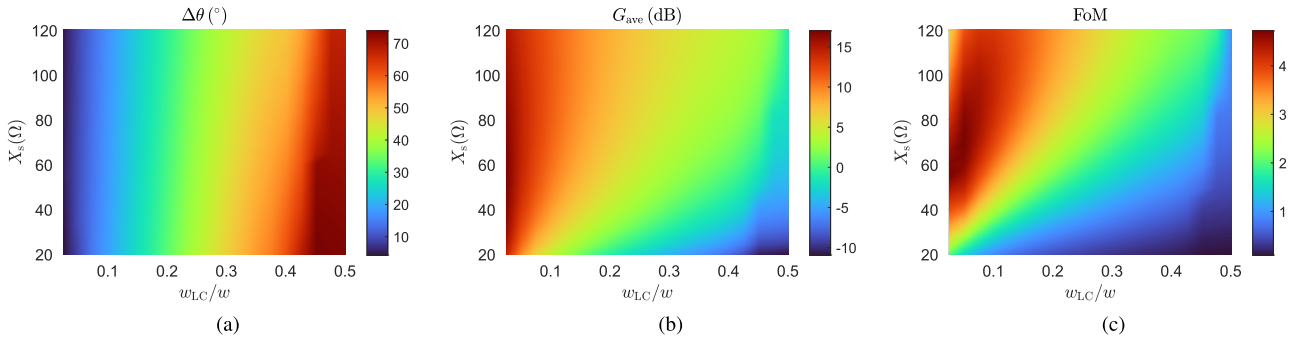

FIGURE 2. (a) Beam-steering angle $\Delta\theta$ (in degrees), (b) average gain G_{ave} (in dBi), and (c) figure of merit (FoM) vs. X_s and the LC ratio w/w_{LC} evaluated at the frequency for which $\beta \simeq 0.95k_0$ in the 'on' state of the LC.

total attenuation constant [41]. For real materials, such as the LC and most dielectric substrates the loss tangent is typically in the range $10^{-3} < \tan\delta < 10^{-2}$. Thus, a few wavelengths are sufficient to radiate most of the accepted power. We then set the antenna length to $L = 10\lambda_0 \simeq 3$ mm.

Second, we notice that w cannot be chosen arbitrarily. In order to have a *fast*, radiating, TE leaky wave, i.e., $0 < \beta < k_0$, the electrical length of the waveguide height should be in the range $0.5/\sqrt{\varepsilon_{\text{eff}}} < w/\lambda_0 < 0.5/\sqrt{\varepsilon_{\text{eff}} - 1}$. This requirement follows from the resonance condition for having the *fundamental* leaky mode radiating at angle θ_0 which reads $w/\lambda_0 \simeq 0.5/\sqrt{\varepsilon_{\text{eff}} - \sin^2\theta_0}$. Here, we set $w = 96\ \mu m$ to have broadside radiation ($\theta_0 = 0°$) in the limit case $w_{LC} \to 0$ and $X_s \to 0$ at the design frequency f_0. This choice will ensure the TE leaky mode to be above cutoff for any combination of w_{LC} and X_s.

A different choice would simply change the beam angle. Still, the beam angle has an impact on the FoM defined in (10): the higher the beam angle, the higher the FoM. Unfortunately, 1-D LWAs are not efficient when radiating too close to endfire, so we disregard design parameters that lead to antenna configurations radiating under these conditions.

At this stage, we are left with three out of five parameters, among which the operating frequency f_{op} is subject to certain physical constraints. Indeed, f_{op} has to be greater than the leaky cutoff (i.e., the frequency for which $\beta > \alpha$) and smaller than the frequency for which $\beta < k_0$. In order to further reduce the dimension of the parameter space and to test the antenna performance in the same operating conditions, we fix f_{op} to the frequency for which $\beta = 0.95k_0$ (that corresponds to $\theta_0 \simeq 72°$) when the LC is in the 'on' state. This condition ensures, for each pair of X_s and w_{LC}/w, that the objective functions are evaluated for LWAs that do not radiate too close to endfire. (Note that when switching to the 'off' state β and in turn θ_0 decrease). A different choice of f_{op} angularly shifts the beam peak according to the frequency-scanning behavior of LWAs. This angular shift, can be compensated by adjusting w, as both the frequency and thickness act in the same way on the leaky phase constant.

As shown in Fig. 2(a)–(c), the angular range, the average gain, and the FoM have been calculated according to (6), (9), and (10), respectively, for a simultaneous variation of X_s and w_{LC}/w. The evaluation of $\Delta\theta$ requires to solve the dispersion equation *twice* for each pair of X_s and w_{LC}/w: the first for the 'on' state and the second for the 'off' state. The evaluation of G_{ave} requires to solve the dispersion equation *four* times for each pair of X_s and w_{LC}/w in order to obtain the leaky wavenumber in the 'on' and 'off' state for both the lossless and the lossy structure; the latter distinction is necessary to evaluate the total efficiency as previously explained in Subsection II-A. Finally, the FoM is obtained by multiplying $\Delta\theta$ and G_{ave}. The results of Fig. 2(a)–(b) show that $\Delta\theta$ mostly depends on w_{LC}/w and is almost independent from X_s, whereas G_{ave} is considerably affected by both w_{LC}/w and X_s increasing for lower values of the former and higher values of the latter. These results are consistent with the theoretical expectation that a higher value of w_{LC}/w improves $\Delta\theta$, but has a detrimental effect on the gain, thus establishing a trade-off, which is clearly revealed by the FoM shown in Fig. 2(c). In particular, it is found that the highest FoM is obtained for $X_s = 70\ \Omega$ and $w_{LC}/w = 0.05$. However, this choice would lead to a very limited tunable range (see Fig. 2(a)). We thus set $w_{LC}/w = 0.2$ to have $\Delta\theta > 25°$. The optimum sheet reactance value for this choice corresponds to around $X_s = 90\ \Omega$. These values are used to synthesize a practical PRS (see Section IV) and to accurately determine the LC dynamics (see Section V) of the antenna prior to the full-wave validation of the entire structure reported in Section VI. As a final remark, we should point out that for the pair $w_{LC}/w = 0.2$ and $X_s = 90\ \Omega$, the working frequency to have $\beta = 0.95k_0$ in the LC 'on' state is $f_{op} = 1.01$ THz. For the sake of convenience we consider $f_{op} = 1$ THz with negligible variations on the antenna performance.

IV. PRS REALIZATION

In [32], it was shown through the equivalence theorem that a 1-D array of transverse slots, when used as a PRS, efficiently couples with the TM leaky mode. By the same token, a 1-D array of longitudinal slots efficiently couples with the antenna under investigation that radiates through the TE leaky mode. For this purpose, we consider a unit-cell consisting of a longitudinal slot at the interface between the spacer and

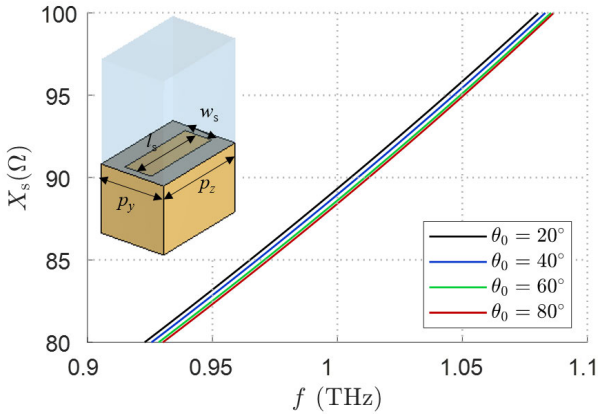

FIGURE 3. Sheet reactance vs. frequency of the longitudinal slot for realizing the PRS (parameters in the text). The CST full-wave simulations are obtained for different angles of incidence in the range $20° \leq \theta_0 \leq 80°$. (Parameters: $p_y = 50\ \mu m$, $p_z = 75\ \mu m$, $w_s = 21\ \mu m$, $l_s = 63\ \mu m$).

the air to simulate the same environment in which the PRS will be inserted. We then consider a rectangular unit cell with $p_y = d \simeq 50\ \mu m$ to match the waveguide short side and $p_z = \lambda_0/4 \simeq 75\ \mu m$ to treat the PRS as a homogenized metasurface in order to fully characterize its electromagnetic response under TE polarization with a scalar sheet impedance. We performed several full-wave simulations by varying both the slot length l_s and width w_s to find a pair of practical values that allowed for synthesizing the required value of $X_s = 90\ \Omega$ at $f_{op} = 1$ THz for an angle of incidence of $\theta_0 = 55°$ (corresponding to the average of the beam angles across the entire tunable range). Full-wave results for $w_s = 21\ \mu m$ and $l_s = 63\ \mu m$ are shown in Fig. 3 over the frequency range 0.9 THz to 1.1 THz, for different angles of incidence in the range $20° \leq \theta_0 \leq 80°$. It is noted that the spatial dispersion of this PRS is remarkably small for the angular range of interest, viz., $40° < \theta_0 < 70°$, thus the reactance values obtained for different angles of incidence within this range will not substantially change, with negligible effects on the antenna optimization.

V. LC DYNAMICS

When zero bias voltage is applied, the nematic LC molecules are oriented along the z-axis by thin polymeric alignment layers (not shown in Fig. 1). The thickness of such layers is in the order of tens of nanometers and their impact in the antenna performance is negligible. The low-frequency (KHz) LC control voltage V_0 is applied between the top and bottom PEC surfaces, as shown in Fig. 1(a). In order to electrically isolate the lateral PEC/PRS walls from the voltage-application electrodes, a small gap has to be introduced by slightly reducing the waveguide thickness d or width w. Given the electric breakdown strength for Zeonor ($E_b > 100$ V/μm [46]), a micron-sized gap is sufficient without perturbing appreciably the THz properties of the leaky mode.

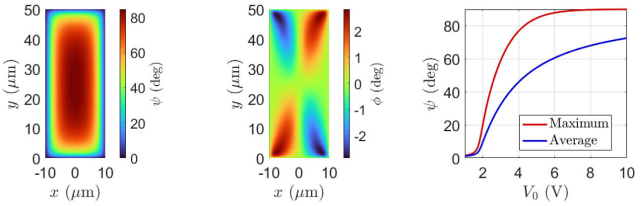

FIGURE 4. (a) Tilt angle profile $\psi(x, y)$ and (b) twist angle profile $\phi(x, y)$ calculated in the LC-filled waveguide for $w = 100\ \mu m$ and $V_0 = 5$ V. (c) Maximum and average tilt angle as a function of the applied voltage.

In the presence of a bias voltage, the molecules of the positive-dielectric anisotropy LC mixture tend to align with the direction of the applied field. Their average local orientation is described by a spatially dependent unit vector, the nematic director $\hat{\mathbf{n}}$. We define the LC tilt angle ψ measured from the z-axis in the zy-plane and the LC twist angle ϕ, measured from the z-axis in the zx-plane. Under this definition the director is expressed as

$$\hat{\mathbf{n}} = \cos\psi \sin\phi \hat{\mathbf{x}} + \sin\psi \hat{\mathbf{y}} + \cos\psi \cos\phi \hat{\mathbf{z}} \qquad (11)$$

such that for zero bias voltage $\psi = \phi = 0$ and $\hat{\mathbf{n}} \equiv \hat{\mathbf{z}}$. The elements ε_{ij} of the LC relative permittivity tensor $\hat{\varepsilon}$ depend on the nematic director via

$$\varepsilon_{ij} = \varepsilon_\perp \delta_{ij} + \Delta\varepsilon n_i n_j \qquad (12)$$

where δ_{ij} is the Kronecker delta, $\Delta\varepsilon = \varepsilon_\perp - \varepsilon_\parallel$, hence the diagonal and anti-diagonal components read $\varepsilon_{xx} = \varepsilon_\perp + \Delta\varepsilon \cos^2\psi \sin^2\phi$, $\varepsilon_{yy} = \varepsilon_\perp + \Delta\varepsilon \sin^2\phi$, $\varepsilon_{zz} = \varepsilon_\perp + \Delta\varepsilon \cos^2\psi \cos^2\phi$, $\varepsilon_{xz} = \varepsilon_{zx} = \Delta\varepsilon \cos^2\psi \sin\phi \cos\phi$, whereas the off-diagonal components read $\varepsilon_{xy} = \varepsilon_{yx} = \Delta\varepsilon \cos\psi \sin\psi \sin\phi$ and $\varepsilon_{yz} = \varepsilon_{zy} = \Delta\varepsilon \cos\psi \sin\psi \cos\phi$.

Although in ideal, planar LC cells the twist angle is zero, in laterally confined finite cavities, such as the one here investigated, the LC molecules are twisted owing to the dielectric permittivity mismatch at the LC/lateral wall interface, which leads to a vertical component of the bias field and hence some twist [47]. However, as far as the antenna analysis is concerned, the twist angle does not play any role. The LWA is designed to operate on the fundamental TE leaky mode, which has a single field component E_y. Hence, the dependence of the antenna properties on the LC orientation is described only by the corresponding ε_{yy} element of the LC permittivity tensor, which is a function of the tilt angle only. This greatly simplifies the analysis.

Figure 4 summarizes the electro-optic behaviour of the investigated LC-filled waveguide. The calculations of the LC orientation profile as a function of the applied voltage V_0 were performed by means of a rigorous tensorial formulation of the Landau–de Gennes theory [48], [49]. Hard anchoring was assumed at all the four LC cavity walls with a pretilt (pretwist) angle of 1°(0°). The elastic constants of the LC mixture 1825 are $K_{11} = 12.5$ pN, $K_{22} = 7.1$ pN, $K_{33} = 32.1$ pN and the low-frequency LC relative permittivities are $\varepsilon_\perp^l =$

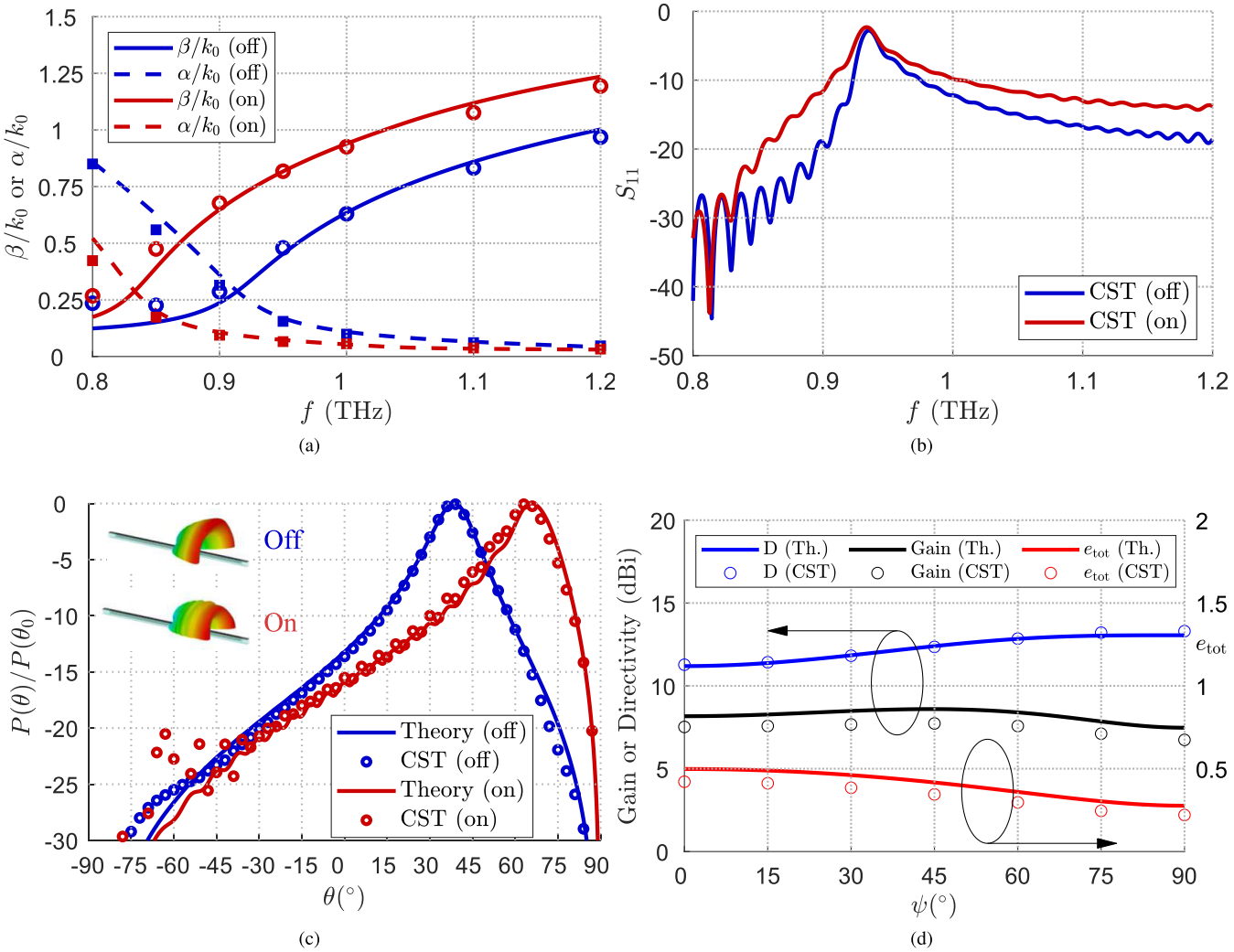

FIGURE 5. (a) Numerically calculated dispersion diagram, (b) S_{11} vs. frequency, (c) normalized far-field patterns for the considered LWA operating in its off (red) and 'on' state (blue), and (d) directivity (blue), gain (black), and efficiency (red) vs. LC tilt angle ψ(°). In (a) circles and squares represent the values of the phase and attenuation constants, respectively, as obtained from CST full-wave simulations. The insets in (c) reproduce the 3-D far-field radiation patterns obtained from CST full-wave simulations at 1 THz. In (d) theoretical and CST results are reported in solid lines and circles, respectively.

4.7 and $\varepsilon_{\parallel} = 21.7$ [36]. Figure 4(a) shows the tilt angle profile $\psi(x, y)$ over the LC cavity cross-section for $V_0 = 5$ V. At the cavity walls the tilt angle is fixed by the anchoring conditions and progressively increases towards the maximum value at the cavity center. The equivalent twist profile $\phi(x, y)$ shows four lobes of alternating sign and low absolute values, as evidenced in Fig. 4(b). The dependence of the maximum and average tilt value as a function of the applied bias voltage is investigated in Fig. 4(c). Switching of the LC molecules occurs above a threshold of approximately 1.5 V. At $V_0 \simeq 6$ V the tilt obtains its maximum value of 90°. The average tilt value increases less steeply due to the anchoring at the cavity walls and reaches 75° for $V_0 = 10$ V. Given the sinusoidal dependence of ε_{yy} on the tilt angle, working in the interval up to 10 V provides almost the entire tunability range for the LWA while keeping single-digit values for the operation voltage.

VI. RESULTS AND DISCUSSION

The in-depth analyses of the previous sections confirm the soundness of the approximations adopted for the LC modeling and the PRS representation that we used to design the antenna. Here, we assess a full-wave validation of the entire three-dimensional (3-D) structure and compare the numerical results with the theoretical expectations. For this purpose, a metallic rectangular leaky waveguide as the one depicted in Fig. 1(a) is designed, with the final parameters reported in Table 1. The cross section of the antenna waveguide (viz., $96\,\mu m \times 53\,\mu m$) matches the dimension of commercially available waveguide transitions (viz., $106\,\mu m \times 53\,\mu m$, WR-0.43) [50] through two linearly tapered extensions of length $\lambda/5 \simeq 60\,\mu m$. These two extensions are entirely filled with Zeonor to encapsulate the LC cell within the waveguide and achieve a good impedance matching. We note that the cutoff frequency of the air-filled waveguide is about 1.4 THz which

TABLE 1. Design parameters.

w	d	L	l_s	w_s
96 μm	50 μm	3 mm	63 μm	21 μm

scales down to about 0.9 THz when considering the Zeonor dielectric filling. Two waveguide ports are then used at the two terminations: one to feed the antenna in its fundamental TE mode, the other one to emulate the effect of an absorber. The 3-D structure is then simulated with the time-domain solver CST Microwave Studio [51]. We obtained from CST a validation of the dispersion properties of the antenna by defining near-field sample locations along a straight line inside the LWA and extracted the attenuation and phase constant from the electric field amplitudes and phases at those samples. As shown in Fig. 5(a), both the phase and attenuation constant retrieved from CST (circles and dots) are in very good agreement with theoretical (solid lines) results obtained by numerically solving for the leaky modes of (1) in the 'off' and 'on' states of the LC (in blue and red, respectively), except for frequency points below the leaky cutoff for which the electromagnetic field is mostly reactive.

We obtained from CST both the S_{11} over the frequency range of interest (see Fig. 5(b)) and the normalized far-field 1-D power patterns (see Fig. 5(c)). The results of Fig. 5(b) show that the insertion loss is lower than -10 dB at the operating frequency of 1 THz, thus having minor effects on the realized gain of the antenna. We should stress that, although the antenna exhibits a good impedance matching over a large bandwidth, the performance is optimized at 1 THz. For a different choice of the frequency the beam peak will scan according to the frequency-scanning behavior of LWAs (see Section III-B) and following the frequency dispersion of the leaky phase contant shown in Fig. 5(a).

In Fig. 5(c) the full-wave patterns (in circles) are compared with the analytical radiation patterns (in solid lines) obtained through (5) when the leaky wavenumbers at 1 THz shown in Fig. 5(a) are used. The agreement is impressive and confirms the expected tunability and directivity. Specifically, the pattern scans an angular range of about 28° going from 38° to 66°, with a beamwidth of about $\Theta_h \simeq 16°$ and exhibiting a directivity (gain) that goes from 11.27(7.52) dBi to 13.30(6.73) dBi, as shown in Fig. 5(d). Although the beam is more directive as the LC state switches from the 'off' to the 'on' state, the gain decreases because of the reduced total efficiency. It should be stressed that CST includes mismatching losses in the evaluation of the total efficiency, which are instead neglected in our theoretical model; this aspect explains the slight disagreement between theoretical and CST results for the gain and the efficiency.

To complete the picture, Table 2 compares the relevant figures of merit obtained in this work with those obtained in [31] and [32] which report similar leaky waveguides based on LC. We should stress the different radiation mechanism

TABLE 2. Performance of LC-based 1-D LWAs.

Ref.	Mode	f_{op}	e_{tot}	Gain	$\Delta\theta$	FoM	LC V_{th}	PMC
[31]	HE_{11}	90 GHz	69%–48%	12 dBi	10°	2.76	>5 V	No
[32]	TM	1.05 THz	71%–60%	11.8 dBi	15°	3.96	10 V	Yes
This Work	TE	1.00 THz	42%–22%	7.4 dBi	28°	2.75	1.5 V	No

of each structure. The dielectric image-line (DIL) [52] LWA in [31] is a 1-D periodic LWA which radiates through the $n = -1$ Floquet harmonic of the perturbed fundamental mode of the DIL (viz., the HE_{11} [53]). The antenna is designed to radiate at approximately 90 GHz with moderate gain and reconfigurability.

The leaky waveguides in [32] and in this work are instead 1-D quasi-uniform LWAs [18], [35] that radiate around 1 THz through the fundamental ($n = 0$) Floquet harmonic due to the deeply subwavelength character of the PRS. In [32] the leaky waveguide is fed in its fundamental TM mode and thus requires two PMC side walls that have a detrimental effect in the biasing scheme that requires threshold voltages larger than 10 V. However, the antenna improves the performance of [31] in terms of reconfigurability (15° in [32] instead of 10° in [31]), while maintaining almost the same gain. This effect allows to reach a relatively large FoM. In this work, we designed the leaky waveguide to operate in its fundamental TE mode so as to avoid the two PMC walls, and greatly improve the performance in terms of reconfigurability (28° here instead of 15° in [32]). This improvement came at the expense of a lower average gain (7.5 dBi here instead of 11.8 dBi in [32]), which further reduced the FoM. This side effect was predictable from the theoretical analysis in Section III, where we highlighted the trade-off between the average gain and the reconfigurable range. Still, the proposed antenna can be designed to maximize the FoM, by choosing a different pair of reactance and LC ratio as shown in Fig. 2(c). In any case, the TE leaky waveguide has the significant advantage of not requiring the synthesis of PMC walls which also leads to a very low threshold voltage and an easier manufacturing process with respect to [32].

In this regard, it is worthwhile to comment on the fabrication of this device. The PRS can be patterned on a ~40-μm Zeonor film using standard photolithography, which amply provides the necessary resolution [54], [55]. The lateral metallic walls do not need to be patterned and they can be supported by a dielectric substrate (not shown in Fig. 1) to provide stability and define laterally the cavity. LC infiltration can occur by capillary action considering the thickness of the LC cavity (~20-μm). Finally the infiltrated antenna can be back-coupled to the reference WR waveguide. Regarding the measurement of the antenna, the frequency-domain THz platform Terascan (Toptica Photonics AG) enriched by an automated stage would represent an ideal measurement setup. The THz signal (obtained from heterodyining the optical

signal from the fibers) coming from the photoconductive antenna can be coupled in free-space to a metallic horn in back-to-back configuration with the WR-0.43 waveguide transition that feeds the leaky waveguide. The amplitude and phase of the *y*-component of the electric field radiated by the LWA can be probed over the aperture plane (a similar technique has been used in [56]), and then used as equivalent radiating current to obtain the far-field pattern through the standard Stratton–Chu radiation integrals [57]. This measurement has to be repeated for any biasing voltage state of interest.

VII. CONCLUSION

We presented an original leaky waveguide operating in its fundamental TE mode. Thanks to the inclusion of a liquid crystal, which is sandwiched between two low-loss dielectric polymers, the device is capable of dynamically steering a rather directive beam (about 16°) over an angular range of about 28°, by applying a relatively low bias voltage (less than 10 V) to the lateral side metallic walls. We took into account the LC dynamics, and designed the radiating aperture so as to obtain the highest gain for the sought tunable angular range. The radiating aperture is then synthesized through a 1-D array of longitudindal slots to efficiently couple with the propagating TE leaky mode. The entire 3-D structure is finally validated with full-wave simulations showing a remarkable agreement when compared against theoretical results based on a simple, yet accurate, model. The efficient biasing scheme and the excellent antenna performance in terms of gain and tunable angular range make the proposed device attractive for future THz antenna applications.

REFERENCES

[1] P. H. Siegel, "Terahertz technology," *IEEE Trans. Microwwave Theory Tech.*, vol. 50, no. 3, pp. 910–928, Aug. 2002.

[2] P. H. Siegel, "Terahertz technology in biology and medicine," *IEEE Trans. Microw. Theory Techn.*, vol. 52, no. 10, pp. 2438–2447, Oct. 2004.

[3] M. Tonouchi, "Cutting-edge terahertz technology," *Nature Photon.*, vol. 1, no. 2, pp. 97–105, Feb. 2007.

[4] H.-J. Song and T. Nagatsuma, "Present and future of terahertz communications," *IEEE Trans. Terahertz Sci. Technol.*, vol. 1, no. 1, pp. 256–263, Sep. 2011.

[5] I. F. Akyildiz, C. Han, Z. Hu, S. Nie, and J. M. Jornet, "Terahertz band communication: An old problem revisited and research directions for the next decade," *IEEE Trans. Commun.*, vol. 70, no. 6, pp. 4250–4285, Jun. 2022.

[6] J. M. Jornet, E. W. Knightly, and D. M. Mittleman, "Wireless communications sensing and security above 100 GHz," *Nature Commun.*, vol. 14, no. 1, p. 841, Feb. 2023.

[7] D. Pirrone, A. Ferraro, D. C. Zografopoulos, W. Fuscaldo, P. Szriftgiser, G. Ducournau, and R. Beccherelli, "Metasurface-based filters for high data rate THz wireless communication: Experimental validation of a 14 Gbps OOK and 104 Gbps QAM-16 wireless link in the 300 GHz band," *IEEE Trans. Wireless Commun.*, vol. 21, no. 10, pp. 8688–8697, Oct. 2022.

[8] C. M. Armstrong, "The truth about terahertz," *IEEE Spectr.*, vol. 49, no. 9, pp. 36–41, Sep. 2012.

[9] E. Torabi, D. Erricolo, P.-Y. Chen, W. Fuscaldo, and R. Beccherelli, "Reconfigurable beam-steerable leaky-wave antenna loaded with metamaterial apertures using liquid crystal-based delay lines," *Opt. Exp.*, vol. 30, no. 16, pp. 28966–28983, 2022.

[10] Y. Monnai, X. Lu, and K. Sengupta, "Terahertz beam steering: From fundamentals to applications," *J. Infr., Millim., THz Waves*, vol. 44, nos. 3–4, pp. 169–211, Apr. 2023.

[11] M. Alonso-delPino, C. Jung-Kubiak, T. Reck, N. Llombart, and G. Chattopadhyay, "Beam scanning of silicon lens antennas using integrated piezomotors at submillimeter wavelengths," *IEEE Trans. THz Sci. Technol.*, vol. 9, no. 1, pp. 47–54, Jan. 2019.

[12] Y. Yang, O. D. Gurbuz, and G. M. Rebeiz, "An eight-element 370–410-GHz phased-array transmitter in 45-nm CMOS SOI with peak EIRP of 8–8.5 dBm," *IEEE Trans. Microw. Theory Techn.*, vol. 64, no. 12, pp. 4241–4249, Dec. 2016.

[13] D. Headland, W. Withayachumnankul, R. Yamada, M. Fujita, and T. Nagatsuma, "Terahertz multi-beam antenna using photonic crystal waveguide and Luneburg lens," *APL Photon.*, vol. 3, no. 12, Dec. 2018, Art. no. 126105.

[14] T. J. Cui, M. Q. Qi, X. Wan, J. Zhao, and Q. Cheng, "Coding metamaterials, digital metamaterials and programmable metamaterials," *Light, Sci. Appl.*, vol. 3, no. 10, p. e218, Oct. 2014.

[15] E. D. Cullens, L. Ranzani, K. J. Vanhille, E. N. Grossman, N. Ehsan, and Z. Popovic, "Micro-fabricated 130–180 GHz frequency scanning waveguide arrays," *IEEE Trans. Antennas Propag.*, vol. 60, no. 8, pp. 3647–3653, Aug. 2012.

[16] S. S. Yao, Y. J. Cheng, Y. F. Wu, and H. N. Yang, "THz 2-D frequency scanning planar integrated array antenna with improved efficiency," *IEEE Antennas Wireless Propag. Lett.*, vol. 20, no. 6, pp. 983–987, Jun. 2021.

[17] D. R. Jackson, P. Burghignoli, G. Lovat, F. Capolino, J. Chen, D. R. Wilton, and A. A. Oliner, "The fundamental physics of directive beaming at microwave and optical frequencies and the role of leaky waves," *Proc. IEEE*, vol. 99, no. 10, pp. 1780–1805, Oct. 2011.

[18] D. R. Jackson, C. Caloz, and T. Itoh, "Leaky-wave antennas," *Proc. IEEE*, vol. 100, no. 7, pp. 2194–2206, Jul. 2012.

[19] B.-Z. Xu, C.-Q. Gu, Z. Li, and Z.-Y. Niu, "A novel structure for tunable terahertz absorber based on graphene," *Opt. Exp.*, vol. 21, no. 20, pp. 23803–23811, 2013.

[20] E. S. Torabi, A. Fallahi, and A. Yahaghi, "Evolutionary optimization of graphene-metal metasurfaces for tunable broadband terahertz absorption," *IEEE Trans. Antennas Propag.*, vol. 65, no. 3, pp. 1464–1467, Mar. 2017.

[21] M. Esquius-Morote, J. S. Gómez, and J. Perruisseau-Carrier, "Sinusoidally modulated graphene leaky-wave antenna for electronic beamscanning at THz," *IEEE Trans. THz Sci. Technol.*, vol. 4, no. 1, pp. 116–122, Jan. 2014.

[22] X.-C. Wang, W.-S. Zhao, J. Hu, and W.-Y. Yin, "Reconfigurable terahertz leaky-wave antenna using graphene-based high-impedance surface," *IEEE Trans. Nanotechnol.*, vol. 14, no. 1, pp. 62–69, Jan. 2015.

[23] W. Fuscaldo, P. Burghignoli, P. Baccarelli, and A. Galli, "Graphene Fabry–Pérot cavity leaky-wave antennas: Plasmonic versus nonplasmonic solutions," *IEEE Trans. Antennas Propag.*, vol. 65, no. 4, pp. 1651–1660, Apr. 2017.

[24] D. C. Zografopoulos, A. Ferraro, and R. Beccherelli, "Liquid-crystal high-frequency microwave technology: Materials and characterization," *Adv. Mater. Technol.*, vol. 4, no. 2, Dec. 2018, Art. no. 1800447.

[25] D. C. Zografopoulos, R. Asquini, E. E. Kriezis, A. d'Alessandro, and R. Beccherelli, "Guided-wave liquid-crystal photonics," *Lab Chip*, vol. 12, no. 19, pp. 3598–3610, 2012.

[26] D. C. Zografopoulos and E. E. Kriezis, "Tunable polarization properties of hybrid-guiding liquid-crystal photonic crystal fibers," *J. Lightw. Technol.*, vol. 27, no. 6, pp. 773–779, Mar. 15, 2009.

[27] M. Roig, M. Maasch, C. Damm, and R. Jakoby, "Liquid crystal-based tunable CRLH-transmission line for leaky wave antenna applications at Ka-band," *Int. J. Microw. Wireless Technol.*, vol. 6, nos. 3–4, pp. 325–330, Jun. 2014.

[28] S. Ma, P. Wang, F. Meng, J. Fu, and Q. Wu, "Electronically controlled beam steering leaky wave antenna in nematic liquid crystal technology," *Int. J. RF Microw. Comput.-Aided Eng.*, vol. 30, no. 6, Jun. 2020.

[29] B.-J. Che, T. Jin, D. Erni, F.-Y. Meng, Y.-L. Lyu, and Q. Wu, "Electrically controllable composite right/left-handed leaky-wave antenna using liquid crystals in PCB technology," *IEEE Trans. Compon., Packag., Manuf. Technol.*, vol. 7, no. 8, pp. 1331–1342, Aug. 2017.

[30] W. Fuscaldo, S. Tofani, D. C. Zografopoulos, P. Baccarelli, P. Burghignoli, R. Beccherelli, and A. Galli, "Tunable Fabry–Pérot cavity THz antenna based on leaky-wave propagation in nematic liquid crystals," *IEEE Antennas Wireless Propag. Lett.*, vol. 16, pp. 2046–2049, 2017.

[31] H. Tesmer, R. Razzouk, E. Polat, D. Wang, and R. Jakoby, "Reconfigurable liquid crystal dielectric image line leaky wave antenna at W-band," *IEEE J. Microw.*, vol. 2, no. 3, pp. 480–489, Jul. 2022.

[32] W. Fuscaldo, D. C. Zografopoulos, F. Imperato, P. Burghignoli, R. Beccherelli, and A. Galli, "Analysis and design of tunable THz 1-D leaky-wave antennas based on nematic liquid crystals," *Appl. Sci.*, vol. 12, no. 22, p. 11770, Nov. 2022.
[33] E. Torabi, D. Erricolo, D. C. Zografopoulos, F. Imperato, P. Burghignoli, A. Galli, R. Beccherelli, and W. Fuscaldo, "Reconfigurable THz 1-D leaky-wave antenna based on liquid crystals and a partially reflecting surface," in *Proc. United States Nat. Committee URSI Nat. Radio Sci. Meeting*, Jan. 2023, pp. 70–71.
[34] W. Fuscaldo, A. Galli, and D. R. Jackson, "Optimization of the radiating features of 1-D unidirectional leaky-wave antennas," *IEEE Trans. Antennas Propag.*, vol. 70, no. 1, pp. 111–125, Jan. 2022.
[35] W. Fuscaldo, A. Galli, and D. R. Jackson, "Optimization of 1-D unidirectional leaky-wave antennas based on partially reflecting surfaces," *IEEE Trans. Antennas Propag.*, vol. 70, no. 9, pp. 7853–7868, Sep. 2022.
[36] M. Reuter, N. Vieweg, B. M. Fischer, M. Mikulicz, M. Koch, K. Garbat, and R. Dąbrowski, "Highly birefringent, low-loss liquid crystals for terahertz applications," *APL Mater.*, vol. 1, no. 1, Jul. 2013, Art. no. 012107.
[37] T. Tamir and A. A. Oliner, "Guided complex waves. Part 1: Fields at an interface," *Proc. Inst. Electr. Eng.*, vol. 110, no. 2, pp. 310–324, 1963.
[38] T. Tamir and A. A. Oliner, "Guided complex waves. Part 2: Relation to radiation patterns," *Proc. Inst. Electr. Eng.*, vol. 110, no. 2, pp. 325–334, 1963.
[39] W. Fuscaldo, P. Burghignoli, and A. Galli, "Genealogy of leaky, surface, and plasmonic modes in partially open waveguides," *Phys. Rev. Appl.*, vol. 17, no. 3, Mar. 2022, Art. no. 034038.
[40] V. Galdi and I. M. Pinto, "A simple algorithm for accurate location of leaky-wave poles for grounded inhomogeneous dielectric slabs," *Microw. Opt. Technol. Lett.*, vol. 24, no. 2, pp. 135–140, Jan. 2000.
[41] W. Fuscaldo, "Rigorous evaluation of losses in uniform leaky-wave antennas," *IEEE Trans. Antennas Propag.*, vol. 68, no. 2, pp. 643–655, Feb. 2020.
[42] W. Fuscaldo, D. R. Jackson, and A. Galli, "A general and accurate formula for the beamwidth of 1-D leaky-wave antennas," *IEEE Trans. Antennas Propag.*, vol. 65, no. 4, pp. 1670–1679, Apr. 2017.
[43] M. Schuhler, R. Wansch, and M. A. Hein, "On strongly truncated leaky-wave antennas based on periodically loaded transmission lines," *IEEE Trans. Antennas Propag.*, vol. 58, no. 11, pp. 3505–3514, Nov. 2010.
[44] W. Fuscaldo, A. Galli, and D. R. Jackson, "Formulas for beam shift and beam narrowing in 1-D leaky-wave antennas due to element pattern," *IEEE Antennas Wireless Propag. Lett.*, vol. 22, no. 7, pp. 1691–1695, Jul. 2023.
[45] A. T. Almutawa, A. Hosseini, D. R. Jackson, and F. Capolino, "Leaky-wave analysis of wideband planar Fabry–Pérot cavity antennas formed by a thick PRS," *IEEE Trans. Antennas Propag.*, vol. 67, no. 8, pp. 5163–5175, Aug. 2019.
[46] Zeon Corporation. *Cyclo-Olefin Polymer: Specialty Plastics*. Accessed: Jun. 3, 2022. [Online]. Available: https://www.zeon.co.jp/en/business/enterprise/resin/cop/
[47] D. C. Zografopoulos, R. Beccherelli, A. C. Tasolamprou, and E. E. Kriezis, "Liquid–crystal tunable waveguides for integrated plasmonic components," *Photon. Nanostruct.-Fundamentals Appl.*, vol. 11, no. 1, pp. 73–84, Feb. 2013.
[48] D. C. Zografopoulos, R. Beccherelli, and E. E. Kriezis, "Beam-splitter switches based on zenithal bistable liquid-crystal gratings," *Phys. Rev. E, Stat. Phys. Plasmas Fluids Relat. Interdiscip. Top.*, vol. 90, no. 4, pp. 1–12, Oct. 2014.
[49] G. Isić, B. Vasić, D. C. Zografopoulos, R. Beccherelli, and R. Gajić, "Electrically tunable critically coupled terahertz metamaterial absorber based on nematic liquid crystals," *Phys. Rev. Appl.*, vol. 3, no. 6, pp. 1–10, Jun. 2015.
[50] VDI Virginia Diodes, Inc. *Waveguide Band Designations*. Accessed: Aug. 22, 2023. [Online]. Available: https://vadiodes.com/images/AppNotes/VDI_Waveguide_Designations.pdf
[51] *CST Studio Suite, Dassault Systemes*. Accessed: Aug. 22, 2023. [Online]. Available: https://www.3ds.com/products-services/simulia/products/cst-studio-suite/
[52] D. D. King and S. P. Schlesinger, "Dielectric image lines," *IEEE Trans. Microw. Theory Techn.*, vol. MTT-6, no. 3, pp. 291–299, Jul. 1958.
[53] K. Solbach and I. Wolff, "The electromagnetic fields and the phase constants of dielectric image lines," *IEEE Trans. Microw. Theory Techn.*, vol. MTT-26, no. 4, pp. 266–274, Apr. 1978.
[54] A. Ferraro, D. C. Zografopoulos, R. Caputo, and R. Beccherelli, "Terahertz polarizing component on cyclo-olefin polymer," *Photon. Lett. Poland*, vol. 9, no. 1, pp. 2–4, 2017.
[55] A. Ferraro, D. C. Zografopoulos, R. Caputo, and R. Beccherelli, "Guided-mode resonant narrowband terahertz filtering by periodic metallic stripe and patch arrays on cyclo-olefin substrates," *Sci. Rep.*, vol. 8, no. 1, p. 17272, Nov. 2018.
[56] Y. Monnai, D. Jahn, W. Withayachumnankul, M. Koch, and H. Shinoda, "Terahertz plasmonic Bessel beamformer," *Appl. Phys. Lett.*, vol. 106, no. 2, pp. 1–15, Jan. 2015.
[57] J. A. Stratton, *Electromagnetic Theory*, vol. 33. Hoboken, NJ, USA: Wiley, 2007.

WALTER FUSCALDO (Senior Member, IEEE) received the B.Sc. and M.Sc. (cum laude) degrees in telecommunications engineering from the Sapienza University of Rome, Rome, Italy, in 2010 and 2013, respectively, and the Ph.D. degree (cum laude) (Doctor Europaeus Label) in information and communication technology (applied electromagnetics curriculum) from the Department of Information Engineering, Electronics and Telecommunications (DIET), Institut d'Électronique et de Télécommunications de Rennes (IETR), Université de Rennes 1, Rennes, France, in 2017, under a cotutelle agreement between the institutions.

In 2014, 2017, 2018, and 2023, he was a Visiting Researcher with the NATO-STO Center for Maritime Research and Experimentation, La Spezia, Italy. In 2016, he was a Visiting Researcher with the University of Houston, Houston, TX, USA. Since July 2017, he has been a Postdoctoral Researcher with the Sapienza University of Rome. In July 2020, he joined the Institute for Microelectronics and Microsystems (IMM), Rome, Italy, as a Researcher of the National Research Council of Italy. His current research interests include propagation of leaky waves, surface waves and plasmonic waves, analysis and design of leaky-wave antennas, generation of localized electromagnetic waves, graphene electromagnetics, metasurfaces, and THz antennas.

Dr. Fuscaldo received several prizes, including the prestigious Young Engineer Prize for the Best Paper presented at the 46th European Microwave Conference, in 2016, and the Best Paper in Electromagnetics and Antenna Theory at the 12th European Conference on Antennas and Propagation, in 2018. He is an Associate Editor of the *IET Microwaves, Antennas and Propagation* and *IET Electronic Letters* and a Topic Editor of *Crystals* (MDPI).

ELAHEHSADAT TORABI received the B.Sc. degree in electrical engineering from the Amirkabir University of Technology (Tehran Polytechnic), Tehran, Iran, in 2013, the M.Sc. degree in electrical engineering-field and waves from Shiraz University, Shiraz, Iran, in 2016, and the Ph.D. degree in electrical engineering-electromagnetics from the University of Illinois at Chicago (UIC), Chicago, IL, USA, in 2022. She is currently an Antenna Engineer with UTVATE, San Francisco, CA, USA. Her research interests include tunable microwave and THz devices, beam-steering antennas, and phased array antennas.

DIMITRIOS C. ZOGRAFOPOULOS received the Ph.D. degree from the Aristotle University of Thessaloniki (AUTH), in 2009. Subsequently, he was an AUTH Postdoctoral Research Fellow and a Postdoctoral Fellow with the Greek States Scholarship Foundation, in 2010; and a Visiting Research Fellow with the Department of Electronics Technology, Carlos III University of Madrid, in 2011. Then, he moved under a Marie-Curie Fellowship to the Institute for Microelectronics and Microsystems, Italian National Research Council, Rome, where he was an Appointed Researcher and a Senior Researcher, in 2011 and 2023, respectively. He is the author or the coauthor of more than 100 scientific articles in international journals, more than 90 presentations in international conferences, and three book chapters. His current research interests include the investigation of strongly resonant metasurfaces, tunable metamaterials, components for THz wave manipulation, and the interaction between electromagnetic waves and liquid crystals.

DANILO ERRICOLO (Fellow, IEEE) received the Laurea degree (summa cum laude) in electronics engineering from Politecnico di Milano, Milan, Italy, and the Ph.D. degree in electrical engineering and computer science from the University of Illinois at Chicago (UIC), Chicago, IL, USA. He is a Professor and the Director of graduate studies with the Department of Electrical and Computer Engineering, the Director of the Andrew Electromagnetics Laboratory, and an Adjunct Professor of bioengineering with UIC. In the Summer of 2009, he was an Air Force Faculty Fellow with the Air Force Research Laboratory, Wright–Patterson Air Force Base, Dayton, OH, USA. He has authored or coauthored more than 310 publications in refereed journals and international conferences. His research interests include antenna design, electromagnetic propagation and scattering, high-frequency techniques, wireless communications, electromagnetic compatibility, the computation of special functions, and magnetic resonance imaging. He is a fellow of AAIA and a University of Illinois Scholar. He was a recipient of the 2023 USNC-URSI Impact Award. He has been chairing the Meetings Committee of the IEEE Antennas and Propagation Society, since January 2023. He has an extensive record of service for the U.S. National Committee (USNC), the International Union of Radio Science (URSI), the Committee of the U.S. National Academies, and the Institute of Electrical and Electronics Engineers (IEEE). In particular, he served as the Chair (2009–2011), the Vice Chair (2006–2008), and the Secretary (2004–2005) of the USNC-URSI Commission E on Electromagnetic Environment and Interference. He was the Chair of the USNC-URSI Ernest K. Smith Student Paper Competition, from 2009 to 2014; the Vice-Chair of the Local Organizing Committee of the XXIX URSI General Assembly, held in Chicago, IL, USA, in August 2008; and the General Chairman of the 2012 IEEE International Symposium on Antennas and Propagation and the USNC-URSI National Radio Science Meeting, held in Chicago, in July 2012. He was an Elected Member of the IEEE AP-S Administrative Committee, from 2012 to 2014; and the Chair of the IEEE AP-S Distinguished Lecturer Program (2015–2016) and the Chicago Joint Chapter of the IEEE AP-S and Microwave Theory and Techniques Society (2011–2016). He has served on more than 50 conference technical program committees, chaired over 70 conference sessions, and organized more than 30 special sessions at international scientific conferences. He was the Editor-in-Chief of the IEEE TRANSACTIONS ON ANTENNAS AND PROPAGATION, from August 2016 to September 2022.

ROMEO BECCHERELLI (Member, IEEE) was born in Plovdiv, Bulgaria, in 1969. He received the Laurea (cum laude) and Ph.D. degrees in electronic engineering from the Sapienza University of Rome, Italy, in 1994 and 1998, respectively. In 1997, he joined as a Postdoctoral Research Assistant with the Department of Engineering Science, University of Oxford, Oxford, U.K. He was an Appointed Researcher, a Senior Researcher, and the Director of research with the Institute for Microelectronics and Microsystems, National Research Council of Italy, Rome, in 2001, 2006, and 2021, respectively. He has been a Principal Investigator in research projects funded by the European Community, the European Space Agency, the Italian Government, and the industry; and the Co-Coordinator of four bilateral projects. He has invented two patents and authored more than 100 scientific articles in international journals, more than 110 conference proceedings papers, and eight book chapters. His initial research interests in liquid crystal display technology have evolved into sensor arrays, photonics and plasmonics based on liquid crystals, metamaterial and metasurface devices, and systems for wireless communications in the microwaves and terahertz frequency ranges. His doctoral thesis was awarded the International Otto Lehman Prize in liquid crystal technology by the University of Karlsruhe, Germany, and the Otto Lehmann Foundation, in 1999.

Open Access funding provided by 'Consiglio Nazionale delle Ricerche-CARI-CARE-ITALY'
within the CRUI CARE Agreement